ELSEVIER

Physics of the Earth and Planetary Interiors 119 (2000) 299–309

PHYSICS OF THE EARTH AND PLANETARY INTERIORS

www.elsevier.com/locate/pepi

Silicon self-diffusion in $MgSiO_3$ perovskite at 25 GPa

Daisuke Yamazaki [a,*], Takumi Kato [b], Hisayoshi Yurimoto [c], Eiji Ohtani [d], Mitsuhiro Toriumi [e]

[a] *Geological Institute, Faculty of Science, University of Tokyo, Bunkyo-ku, Tokyo 113-0033, Japan*
[b] *Institute of Geoscience, University of Tsukuba, Tsukuba, Ibaraki 305-8571, Japan*
[c] *Department of Earth and Planetary Sciences, Tokyo Institute of Technology, Meguro-ku, Tokyo 152-8551, Japan*
[d] *Institute of Mineralogy, Petrology and Economic Geology, Tohoku University, Aoba-ku, Sendai 980-8578, Japan*
[e] *Geological Institute, Faculty of Science, University of Tokyo, Bunkyo-ku, Tokyo 113-0033, Japan*

Received 16 August 1999; accepted 3 January 2000

Abstract

Silicon self-diffusion coefficients in $MgSiO_3$ perovskite were measured under lower mantle conditions. The $MgSiO_3$ perovskite was synthesized and diffusion annealing experiments were conducted at pressure of 25 GPa and temperature of 1673–2073 K using a MA8 type high-pressure apparatus. The diffusion profiles were obtained by secondary ion mass spectrometry. The lattice and grain boundary diffusion coefficients (D_1 and D_{gb}) were determined to be $D_1\,[m^2/s] = 2.74 \times 10^{-10}\exp(-336\,[kJ/mol]/RT)$ and $\delta D_{gb}\,[m^3/s] = 7.12 \times 10^{-17}\exp(-311\,[kJ/mol]/RT)$, respectively, where δ is the width of grain boundary, R is the gas constant and T is the absolute temperature. These diffusion coefficients play a key role for understanding the rheology of the lower mantle.

Keywords: Silicon diffusion profile; $MgSiO_3$ perovskite; High pressure and temperature; Rheology of the lower mantle

1. Introduction

Dynamics of earth's interior depends on the rheological properties of its constituent materials. In the earth's lower mantle, (Mg,Fe)SiO_3 perovskite and (Mg,Fe)O magnesiowüstite are believed to be dominant, and perovskite may exceed 85% of the volume (Stixrude et al., 1992). Therefore, the rheological property of perovskite is important for understanding the dynamics of the lower mantle. Plastic deformation of rocks occurs either by motion of dislocations (dislocation creep) or by the diffusive transport of individual atoms (diffusion creep). Based on the experimental studies of lattice preferred orientation and seismological observation (Karato, 1988; Karato and Li, 1992; Meade et al., 1995; Li et al., 1996; Garnero and Lay, 1997), Karato et al., 1995 suggested that diffusion creep (Nabarro–Herring or Coble creep) may dominate in the most part of lower mantle.

In the case of diffusion creep, the viscosity of a material is directly related to its diffusion coeffi-

* Corresponding author. Now at the Department of Geology and Geophysics, University of Minnesota, Minneapolis, MN55455, USA.

E-mail addresses: daisuke@geol.s.u-tokyo.ac.jp, yamaz002@tc.umn.edu (D. Yamazaki), tkato@arsia.geo.tsukuba.ac.jp (T. Kato), yuri@geo.titech.ac.jp (H. Yurimoto), ohtani@mail.cc.tohoku.ac.jp (E. Ohtani), tori@geol.s.u-tokyo.ac.jp (M. Toriumi).

0031-9201/00/$ - see front matter
PII: S0031-9201(00)00135-7

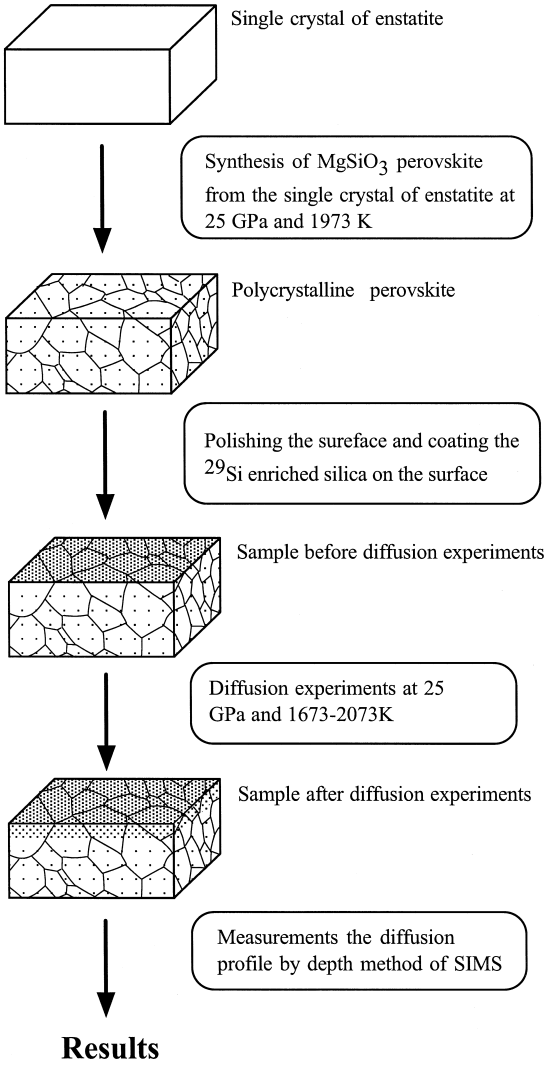

Fig. 1. Flow chart of experimental procedure. A single crystal of pure enstatite transforms to polycrystalline $MgSiO_3$ perovskite due to nucleation and growth. See text in detail.

cients (Frost and Ashby, 1982) and therefore the experimental studies of diffusion coefficients provide important constraints on viscosity. In most silicates, silicon is the slowest diffusing species, and therefore, the diffusion of silicon is likely to control the viscosity in the diffusion creep regime (Jaoul et al., 1981; Houlier et al., 1990; Béjina and Jaoul, 1996; Fisler et al., 1997).

In spite of the importance of silicon diffusion in $MgSiO_3$, the diffusion data have never been reported. It is difficult to determine the diffusion coefficients of $MgSiO_3$ perovskite because $MgSiO_3$ perovskite is stable only at high pressure ($\gtrsim 24$ GPa) and the diffusivity of silicon may be slow, therefore, sensitive analysis to short length of diffusion penetration is needed for measurements of diffusion profiles. Using the advanced high pressure experimental technique and sensitive ion mass analytical method developed by previous workers (e.g., Giletti et al., 1978; Yurimoto and Sueno, 1984; Ito and Takahashi, 1989), we determined the self-diffusion coefficients of silicon in $MgSiO_3$ perovskite under lower mantle conditions.

2. Experimental procedure

We first synthesized $MgSiO_3$ perovskites at 25 GPa and 1973 K from single crystals of synthetic pure enstatite ($0.7 \times 0.7 \times 0.4$ mm^3), using a double-stage multianvil (MA) high-pressure system consisting of an outer MA6 and inner MA8 assembly at Tohoku University (MAP3000) (Ohtani et al., 1998) (Fig. 1). To generate the high pressure up to ~ 25 GPa, an inner MA8 assembly is composed of 26-mm edge cubes with a 2.0 mm of truncated edge length. The initial starting materials of single crystals of enstatite without crack nor inclusion were selected

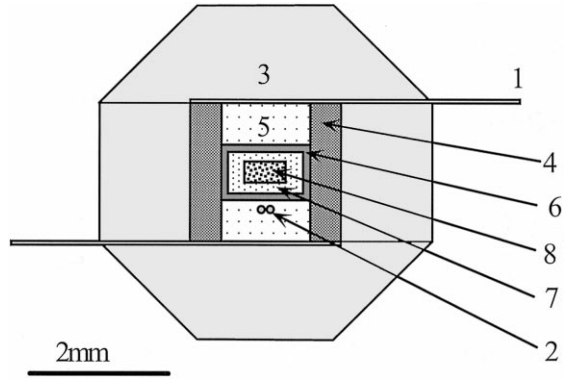

Fig. 2. Furnace assembly for synthesis and diffusion annealing experiments at high pressure and temperature. Eight WC anvils with a 2.0 mm of truncated edge length were used. (1) Mo electrode, (2) $WRe_{3\%}-WRe_{25\%}$ thermocouple, (3) ZrO_2 pressure medium, (4) lanthanum chromite heater, (5) (Mg,Co)O insulator, (6) graphite capsule, (7) NaCl medium, (8) enstatite or pervoskite sample.

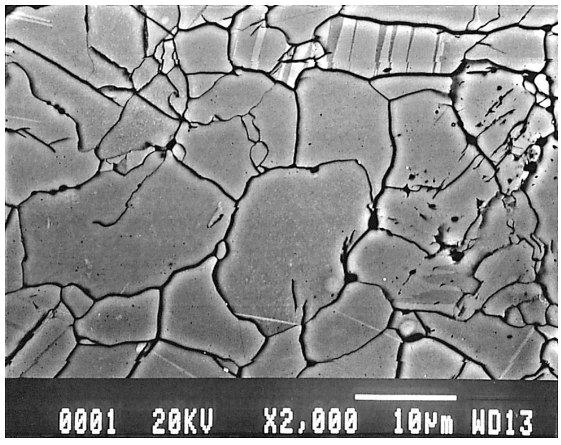

Fig. 3. Back scattered electron image of the sample before diffusion annealing etched by HF for a few second. Twinning were observed.

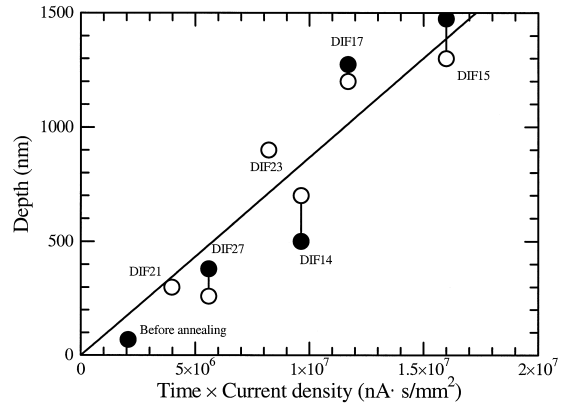

Fig. 4. Crater depth of each samples measured by a surface profiler (open circles) and/or a multibeam interferometer (solid circles) as function of the product of sputtering time and unit primary ion current. Solid line is fit of all data.

under an optical microscope. A graphite capsule and lanthanum chromite heater were used for the furnace assembly, and $WRe_{3\%}$–$WRe_{25\%}$ thermocouples were located in the furnace to monitor the temperature (Fig. 2).

The recovered sample was polycrystalline perovskite (Fig. 3). The grain size ranged from a few to ~20 μm. Some grains show the twin boundaries and grain distribution is homogeneous. Grain boundaries are wavy presumably due to the presence of twin boundaries (Fig. 3). The samples were polished with diamond paste (0.25 μm in diameter). After cleaning with acetone and alcohol, the polished surface was coated with a ^{29}Si-enriched thin film (about 20–30 nm thickness by high vacuum thermal evaporation of a ^{29}Si enriched SiO_2 powder with atomic ratio of isotope of ^{28}Si:^{29}Si:$^{30}Si = 4.12:95.65:0.23$). To confirm the crystallinity of the surface layer of

Table 1
Experimental conditions and results of estimated diffusion coefficients
All experiments were conducted at 25 GPa, which corresponds to ~700 km depth in the earth's mantle. The temperatures and durations for diffusion annealing are shown. The initial and final grain size of perovskite were about 5–20 μm. No significant grain growth was observed during annealing.
Numbers in parentheses represent the uncertainties of diffusion coefficients including the uncertainty of the measured depth and of the fit to diffusion models. Uncertainty of δD_{gb} for run no. DIF 15 does not include the uncertainty of lattice diffusion coefficient.

Run no.	Temperature (K)	Time (h)	D_1^* (m^2/s)	δD_{gb}^{**} (m^3/s)	$-(d\ln(c-c_0))/(dy^{6/5})^{***}$
DIF15†	1673	10	–	$2.47\left(^{+1.29}_{-0.85}\right)\times10^{-26}$	$11.36\left(^{+3.26}_{-2.54}\right)\times10^{-7}$
DIF23	1773	50	$5.29\left(^{+19.3}_{-4.15}\right)\times10^{-20}$	$3.54\left(^{+34.1}_{-3.20}\right)\times10^{-26}$	$9.63\left(^{+15.44}_{-5.56}\right)\times10^{-7}$
DIF27	1873	5	$1.15\left(^{+1.95}_{-0.72}\right)\times10^{-19}$	$1.36\left(^{+6.11}_{-1.11}\right)\times10^{-25}$	$10.79\left(^{+11.45}_{-5.56}\right)\times10^{-7}$
DIF14	1873	10	$9.90\left(^{+1.32}_{-5.65}\right)\times10^{-19}$	$2.36\left(^{+5.12}_{-1.62}\right)\times10^{-25}$	$6.02\left(^{+3.29}_{-2.13}\right)\times10^{-7}$
DIF17	1973	6	$4.30\left(^{+10.3}_{-3.03}\right)\times10^{-19}$	$5.76\left(^{+11.9}_{-3.88}\right)\times10^{-25}$	$6.39\left(^{+2.28}_{-1.68}\right)\times10^{-7}$
DIF21	2073	1	$1.23\left(^{+0.95}_{-0.53}\right)\times10^{-18}$	$7.20\left(^{+26.8}_{-5.67}\right)\times10^{-25}$	$13.12\left(^{+14.81}_{-6.98}\right)\times10^{-7}$

*Lattice diffusion coefficient.
**D_{gb} is grain boundary diffusion coefficient, δ is the width of grain boundary.
***See Eq. (2) in text.
†D_1 was not determined because the run duration was too short. δD_{gb} was estimated by substituting $D_1 = 8.93\times10^{-21}$ at 1673 K, which was obtained by extrapolation of the Arrhenius relationship in Fig. 8A.

samples after polishing before coating, we used EBSP (electron backscattered pattern) technique. We observed Kikuchi bands from our sample (using 30 kV accelerating voltage). This observation indicated that the surface layer is crystalline rather than amorphous at the surface region even less than ~50 nm because the image of Kikuchi band by EBSP is derived from the surface of sample less than ~50 nm (Lloyd et al., 1981; Davies and Randle, 1996; Ren et al., 1998). The coated polycrystalline aggregates of perovskite were used as starting materials of the diffusion annealing experiments. They were pressurized up to 25 GPa at room temperature and then heated at a constant rate of 500°C per min up to the annealing temperature (1673–2073 K) to prevent diffusion during increasing temperature. Constant temperature was kept within 5°C–10°C of the desired value for 1 to 50 h (Table 1). The sample was inside a NaCl pressure medium in order to minimize the differential stress in the synthesis and diffusion experiments (Fig. 2). After the diffusion experiment, the recovered charges were washed by pure water to remove NaCl and to expose the $^{29}SiO_2$ film coated surface. The washed run charges were mounted in

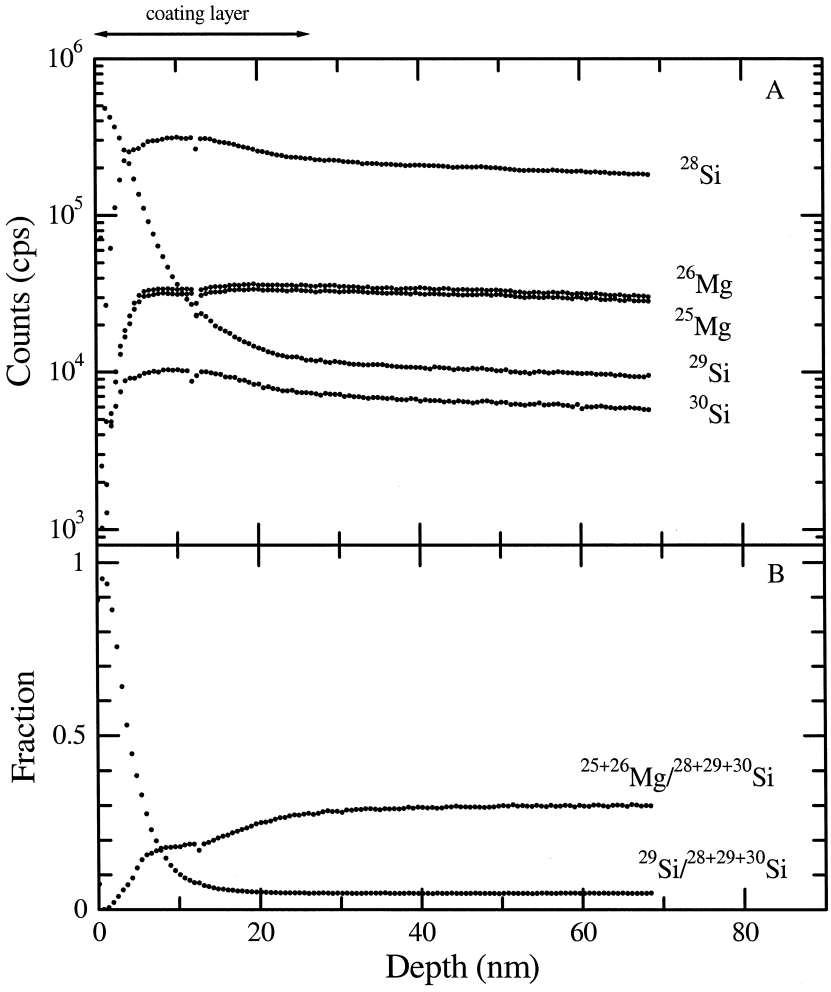

Fig. 5. Secondary ion intensities of $MgSiO_3$ perovskite before annealing as a function of depth from the surface of sample. (A) The counts by SIMS of masses 25 and 26 of Mg, and 28, 29 and 30 of Si were plotted. (B) Ratios of $^{25+26}Mg/Si_{total\ (28+29+30)}$ and $^{29}Si/Si_{total}$. Note that both ratios in deeper portion than ~30 nm are constant. An arrow indicates the range of coating layer.

epoxy disks to analyze diffusion profile of ^{29}Si by a secondary ion mass spectrometry (SIMS). The final grain size of $MgSiO_3$ perovskite aggregates were less than ~ 20 μm, indicating that grain growth did not occur during annealing experiments.

The diffusion profiles of ^{29}Si from the coated surface of $MgSiO_3$ perovskite aggregates were obtained by depth profiling analysis with a rastered primary O^- beam with accelerating voltage of 12.5 kV in the modified Cameca ims3f SIMS instrument at Tokyo Institute of Technology (Yurimoto et al., 1989). Secondary ion intensities from the central area (60 μm in diameter) of sputtered crater (150 μm square) were collected in order to eliminate crater edge effect. The depth calibration of the craters was carried out with a surface profiler and/or a multibeam interferometer after SIMS measurements (Fig. 4). From the relationship between the depth of the crater and the product of sputtering time and current density shown in Fig. 4, the measured depth included $\lesssim 15\%$ relative error. In all measurements, at least 5 masses of ^{25}Mg, ^{26}Mg, ^{28}Si, ^{29}Si and ^{30}Si were detected to estimate the ratio of Mg/Si. Further qualitative analyses were made on some samples

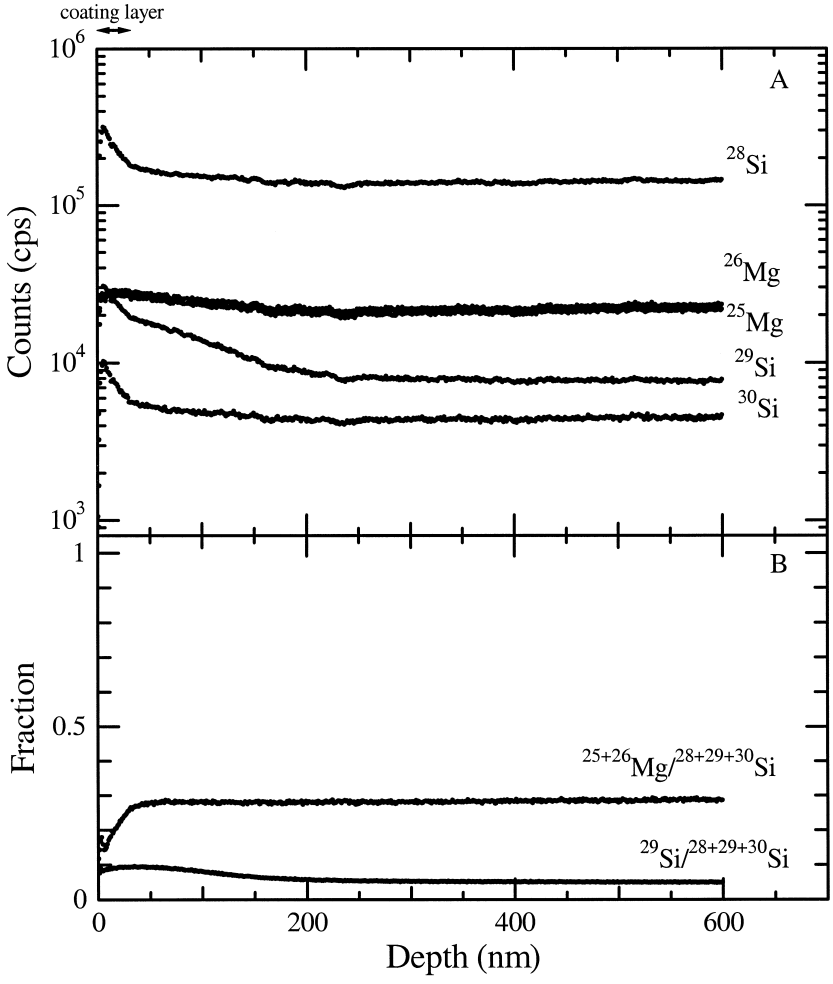

Fig. 6. Secondary ion intensities of $MgSiO_3$ perovskite after annealing at 25 GPa and 1873 K for 10 h as a function of depth from the surface of sample (run no. DIF14). (A) The counts by SIMS of masses 25 and 26 of Mg, and 28, 29 and 30 of Si were plotted. (B) Ratios of $^{25+26}Mg/Si_{total}$ and $^{29}Si/Si_{total}$. Note that $^{25+26}Mg/Si_{total}$ ratios in deeper portion than ~ 30 nm are constant. On the other hand, $^{29}Si/Si_{total}$ ratio decreases with depth, indicating the diffusion process. An arrow indicates the range of coating layer.

to evaluate the contamination during experiments. Figs. 5 and 6 show representative results obtained by depth profiling for sample before and after annealing, respectively. ^{29}Si concentration, c, is represented by the ratio of ^{29}Si/total Si calculated from $I_{29}/(I_{28}+I_{29}+I_{30})$, where I is the secondary ion intensity (counts per second).

3. Diffusion results

Before annealing experiments, the ^{29}Si-profile of a coated sample was measured by SIMS to confirm the condition of thin film (Fig. 5). It was observed that the coated $^{29}SiO_2$ did not penetrate into the polycrystalline perovskite, indicating that the profiles obtained after annealing (Fig. 6) was formed by the diffusion process in $MgSiO_3$ perovskite during annealing. Moreover, the constant Mg/Si ratios with depth after annealing (Fig. 6B) indicate that the mass was transported by the diffusion process without any reaction between the ^{29}Si enriched silica surface layer and perovskite.

When the annealing time was short, the penetration depth was shallow and the profile was characterized by a single curve, suggesting a single diffusion mechanism. On the other hand, when the annealing time was longer, the profiles displayed the pattern which is composed of two segments (Fig. 7). Such a change in the shape of penetration curve is often observed for the diffusion in polycrystalline materials (Harrison, 1961; Atkinson and Taylor, 1979; Farver and Yund, 1991; Farver et al., 1994). One segment near the surface is interpreted as due to the lattice diffusion and the other segment in the deep inside is due to grain boundary diffusion. This suggests that the diffusion regime in our experiments corresponds to the type B as described in Harrison (1961) except for run no. DIF15. Generally, when the condition of $(D_1t)^{1/2} \geq G/2$ is satisfied where D_1 is lattice diffusion coefficient, t is annealing time and G is grain size, a penetration profile can be characterized by a single diffusion coefficient D_A ($D_A=(1-f)D_1+fD_{gb}$, where f is the fraction of materials near grain boundaries where diffusion is enhanced) which represents the effective (bulk) diffusion coefficient. A single curve of penetration profile due to grain boundary diffusion is displayed when the annealing time is so short that $(D_1t)^{1/2} \ll \delta$ (DIF15). The type B diffusion occurs at the condition of $\delta \ll (D_1t)^{1/2} \leq G/2$ and both lattice (shallow region) and grain boundary (deeper region) diffusion play an important role. In the present study, all experiments were conducted at the condition of type B, except for run no. DIF15. Therefore, we were able to determine both lattice and grain boundary diffusion coefficients separately, except for run no. DIF15 in which the concentration curve was almost represented by a single curve due to grain boundary diffusion.

In type B regime, the lattice diffusion segment can be fitted by the following equation in the case of a thin film reservoir of diffusant (Crank, 1975) (Fig. 7A),

$$c - c_0 = \frac{M}{\sqrt{\pi D_1 t}} \exp\left(-\frac{y^2}{4D_1 t}\right) \quad (1)$$

where c is the concentration of ^{29}Si at depth y, c_0 is the initial concentration of ^{29}Si in perovskite and M is the amount of substance deposited at surface. The grain boundary diffusion segment in the ^{29}Si profile was analyzed using the following grain boundary diffusion model (Le Claire, 1963) (Fig. 7B),

$$\delta D_{gb} = 0.66\left(-\frac{\mathrm{d}\ln(c-c_0)}{\mathrm{d}y^{6/5}}\right)^{-5/3}\left(\frac{4D_1}{t}\right)^{1/2} \quad (2)$$

Eq. (2) is insensitive to the boundary structure of a polycrystal during diffusion experiments (Atkinson and Taylor, 1979). The typical fit of Eqs. (1) and (2) to the measured profile are shown in Fig. 7, and results are summarized in Table 1. As shown in Fig. 7, the uncertainty in fits is not large so that this uncertainty does not significantly affect the calculated values of the diffusion coefficients. The uncertainties on diffusion coefficients given in Table 1 are mainly caused by the measurements error on the crater depth. We assumed that the error on the crater depth was given by the difference between the measured depth by a surface profiler and/or multibeam interferometer and the depth calculated from the regression line in Fig. 4.

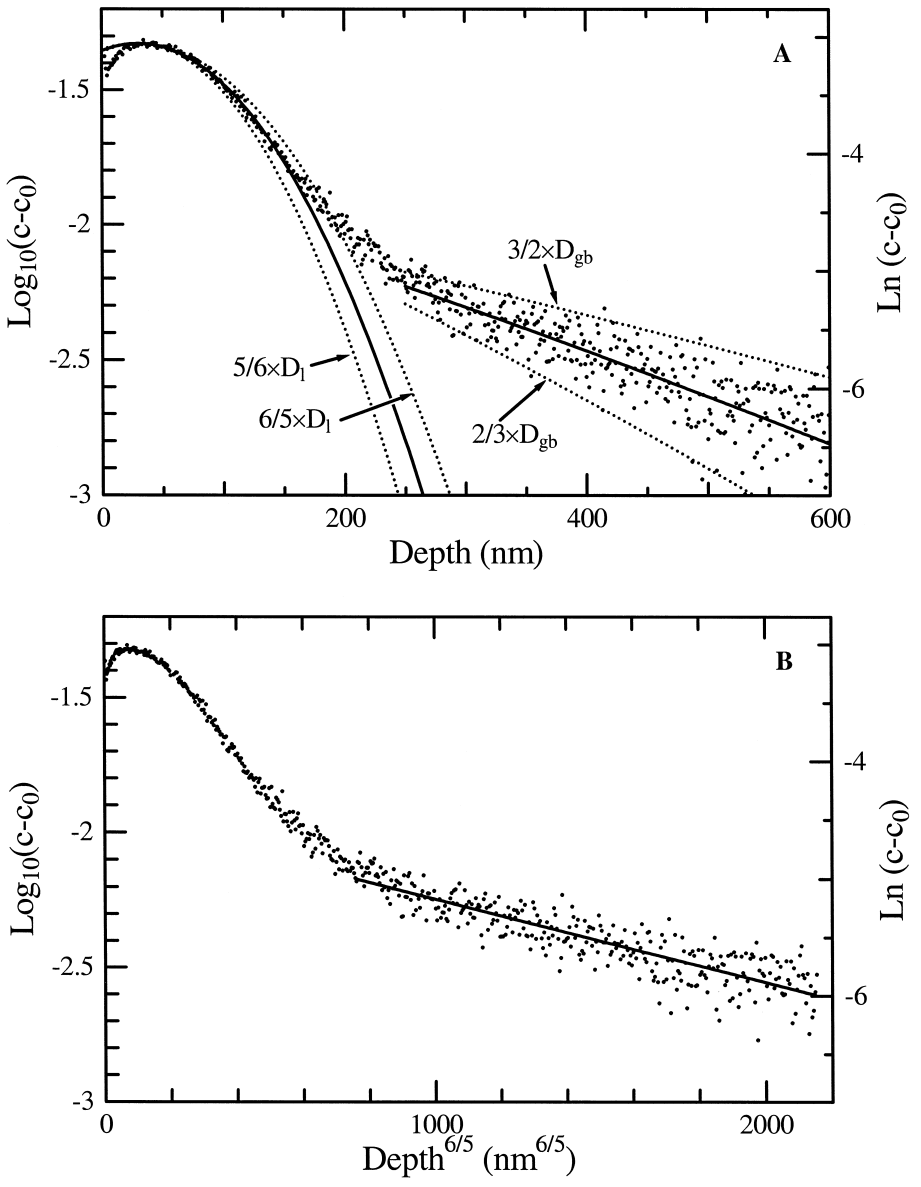

Fig. 7. A diffusion profile of ^{29}Si in perovskite, which was annealed at 25 GPa and 1873 K for 10 h (run no. DIF14), c is $^{29}Si/Si_{total}$ and c_0 is the initial $^{29}Si/Si_{total}$ ratio. (A): The surface region ($\sim$30 nm) corresponds to a coated layer of enriched silica. The depth between $\sim$30 and $\sim$150 nm is the region where lattice diffusion is dominant and between $\sim$260 and $\sim$600 nm is the region where grain boundary diffusion is dominant (see B). Solid dots represent the data obtained by SIMS, solid lines represent the best fit to the lattice diffusion model (Eq. 1) for the measured profile of the lattice diffusion contribution and the best fit to grain boundary diffusion model (Eq. 2) for the measured profile of the region of grain boundary diffusion contribution, respectively. Dashed lines represent model profiles using 5/6 and $6/5 \times D_l$ of the best fit and model profiles using 2/3 and $3/2 \times D_{gb}$ values of the best fit, respectively. (B): Data from (A) plotted as a logarithm of $(c - c_0)$ versus $y^{6/5}$ (where y is the depth) consistent with Eq. (2). Note that the deeper region than $\sim$800 nm$^{6/5}$ corresponding to the depth of $\sim$260 nm yields a straight line over that region of the depth profile where grain boundary diffusion is dominant.

4. Discussion

The diffusion coefficients depend on temperature as $D = D_0 \exp(-H^*/RT)$, where D_0 is the pre-exponential factor, H^* is the activation enthalpy, R is the gas constant and T is the absolute temperature. The pre-exponential factor and activation enthalpy of D_1 are calculated to be $\binom{+24.8}{-2.47} \times 10^{-10}$ m^2/s and $H_1^* = 336(\pm 37)$ kJ/molrespectively (Fig. 8A), and those of δD_{gb} are calculated to be $\binom{+144}{-6.78} \times 10^{-10}$ m^3/s and $H_{gb}^* = 311(\pm 48)$ kJ/mol, respectively (Fig. 8B). If the width of grain boundary can be assumed to be $\sim 10^{-9}$–10^{-10} m (Atkinson and Taylor, 1979; Ricoult and Kohlstedt, 1983; Farver et al., 1994), the grain boundary diffusion is about ~ 4 orders of magnitude faster than the lattice diffusion. The high diffusivity along grain boundary is consistent with the observations in other oxides and silicate crystal (Turnbell and Hoffman, 1954; Yurimoto et al., 1992; Sakaguchi and Haneda, 1996; Farver and Yund, 1995). Although Stocker and Ashby (1973) considered that the relationship between the activation enthalpy for lattice diffusion and that for grain boundary is $H_1^*/H_{gb}^* \sim 1.5$, in the present study we obtain the ratio of ~ 1.1. Similarly, Farver et al. (1994) reported that the activation enthalpy for magnesium grain boundary diffusion in forsterite was only slightly less than that for lattice diffusion.

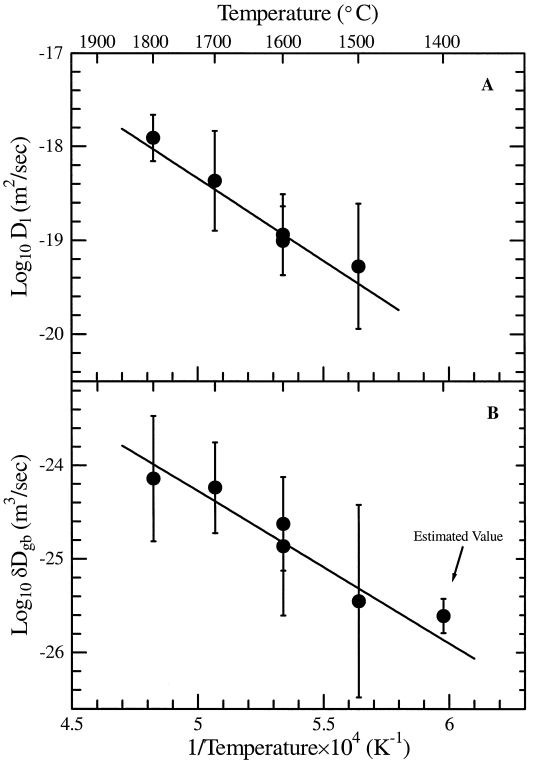

Fig. 8. Silicon self-diffusion coefficients in $MgSiO_3$ perovskite are plotted against inverse temperature. Solid circles represent the lattice diffusion coefficients (A), and the products of the grain boundary diffusion coefficients and the width of grain boundary (B). The error bars show the uncertainties for diffusion coefficients (Table 1). Solid lines represent the least square fits to the data, except for the data point marked by arrow which is estimated value (run no. DIF15, see Table 1).

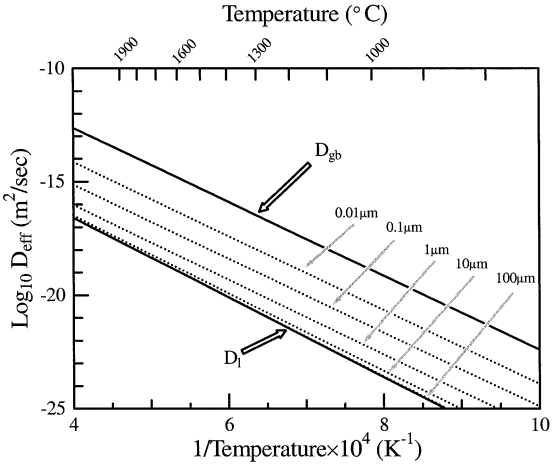

Fig. 9. Effective diffusion coefficients of silicon in $MgSiO_3$ perovskite calculated from the lattice and grain boundary diffusion coefficients (solid lines). Dotted lines represent the effective diffusion coefficients with each grain sizes (0.01–100 μm). The width of grain boundary was assumed to be 10^{-10} m for the estimation of D_{gb}.

In polycrystalline materials, mass transportation is controlled by the effective diffusion coefficient, $D_{eff} = D_1 + \pi\delta D_{gb}/G$, where G is grain size (Raj and Ashby, 1971; Gordon, 1985). We calculated the effective diffusion coefficients for a range of grain size. At the temperature range of lower mantle ($\gtrsim$ 1873 K), the effective diffusion of silicon in perovskite is almost represented by the lattice diffusion if the grain size is larger than a few tens micrometers (Fig. 9). We compare our present results with previous results of diffusion of silicon (Fig. 10). As shown in Fig. 10, the pre-exponential factor and activation enthalpy for lattice diffusion in $MgSiO_3$

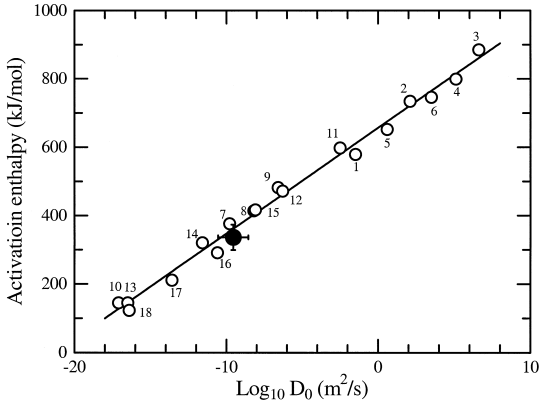

Fig. 10. Linear relationship between pre-exponential factors ($\log D_0$) and activation enthalpy for silicon diffusion in some silicate materials, representing compensation law, modified after Béjina and Jaoul (1997). Numbered open circles display the diffusion data from previous studies and solid circle represent our data. The solid line shows the regression line as H^* [kJ/mol] = $656.6 + 30.9 \times \log D_0$ [m^2/s], including our result. For previous data, (1) vitreous silica (Brébec et al., 1980); (2) synthetic quartz (Jaoul et al., 1995); (3–6) synthetic quartz (Béjina and Jaoul, 1996); (7) forsterite (Jaoul et al., 1981); (8–15) forsterite (different crystallographic direction and buffering materials) (Andersson et al., 1989); (16) San Carlos olivine (Houlier et al., 1990); (17–18) diopside (Béjina and Jaoul, 1996).

perovskite are consistent with the existing data set of silicon diffusion in various silicates (Béjina and Jaoul, 1997). This indicates that the compensation law (Béjina and Jaoul, 1997) for diffusion of silicon for various silicate is applicable to the six-coordinated silicon such as perovskite. We also compare the g-factor defined by $g = H^*/RT_m$, where T_m is melting temperature. The g-factor for silicon diffusion in $MgSiO_3$ perovskite is ~ 14, which is in the smaller end of g-factors in other silicates (~ 10–50) (Jaoul et al., 1981, 1983, 1995; Béjina and Jaoul, 1996; Andersson et al., 1989; Brébec et al., 1980). We suppose that this small g-factor for silicon diffusion in perovskite could be the result of weaker bond strength of six-coordinated silicon than four-coordinated silicon (Gibbs et al., 1998). A weaker bond strength of six-coordinated silicon than four-coordinated silicon is also consistent with the observed negative Clapeylon slope for the perovskite forming reactions (Akaogi and Ito, 1993).

Note that there are some differences between our experimental conditions and conditions in the lower mantle. First, our samples were in contact with SiO_2 and therefore the SiO_2 activity is fixed around the SiO_2-rich end in the SiO_2–(Fe,Mg)O system. As shown in Fig. 5B, the ratio of Mg/Si equals to zero at the surface before annealing. In contrast, this ratio at the surface after annealing is higher than zero (Fig. 6B), suggesting that the coated silicon seems to have been dissolved into $MgSiO_3$ perovskite in a thin surface layer (Fig. 6B). This implies that our $MgSiO_3$ perovskites have SiO_2-excess stoichiometry as opposed to (Mg,Fe)O-excess stoichiometry which is likely the case in earth's lower mantle. The existing experimental data on the effects of oxide activity on silicon diffusion in olivine, however, indicate that the effects of oxide activity are not very large (factor of ~ 5, Andersson et al., 1989). Second, our sample is free from Fe and Al, whereas perovskite in the lower mantle likely contains significant amount of Fe and Al (McCammon, 1997; Wood and Rubie, 1996), which may affect point defect chemistry and hence diffusion. Further studies are needed to access these issues.

Acknowledgements

We greatly thank S. Karato for encouragement, useful discussions and some experimental supports. I am indebted to K. Onuma for the useful discussions, A. Suzuki and M. Ito for the experimental supports, K. H. Lee for technical supports of EBSP works, H. Horiuchi for the use of the micro-area X-ray diffractometer and M. Ozima for providing enstatite. O. Jaoul and an anonymous referee are thanked for their reviewing. D. Yamazaki has been supported by Research Fellowships of the Japan Society for the Promotion of Science for Young Scientists.

References

Akaogi, M., Ito, E., 1993. Refinement of enthalpy measurement of $MgSiO_3$ perovskite and negative pressure–temperature slopes for perovskite forming reactions. Geophys. Res. Lett. 20, 1839–1842.

Andersson, K., Borchart, G., Scherrer, S., Weber, S., 1989. Silicon diffusion in Mg_2SiO_4 at high temperature: a model case study for SIMS analyses on ceramic surface. Fresenius' Z. Anal. Chem. 333, 383–385.

Atkinson, A., Taylor, R.I., 1979. The diffusion of Ni in bulk and along disclocation in NiO single crystals. Philos. Mag. A39, 581–595.

Béjina, F., Jaoul, O., 1996. Silicon self-diffusion in quartz and diopside measured by nuclear micro-analysis methods. Phys. Earth Planet. Inter. 97, 145–162.

Béjina, F., Jaoul, O., 1997. Silicon diffusion in silicate minerals. Earth Planet. Sci. Lett. 153, 229–238.

Brébec, G., Seguin, R., Sella, C., Bevenot, J., Martin, J.-C., 1980. Diffusion du silicium dans la silice amorphe. Acta Metall. 28, 327–333.

Crank, J., 1975. In: The Mathematics of Diffusion. 2nd edn. Clarendon Press, Oxford, pp. 11–27, Chap. 2.

Davies, R., Randle, V., 1996. Secondary processing of electron backscatter data from an aluminum alloy. Mater. Charact. 37, 131–141.

Farver, J.R., Yund, R.A., 1991. Measurement of oxygen grain boundary diffusion in natural, fine-grained, quartz aggregates. Geochim. Cosmochim. Acta. 55, 1597–1607.

Farver, J.R., Yund, R.A., 1995. Grain boundary diffusion of oxygen, potassium and calcium in natural and hot-pressed feldspar aggregates. Contrib. Mineral. Petrol. 118, 340–355.

Farver, J.R., Yund, R.A., Rubie, D.C., 1994. Magnesium grain boundary diffusion in forsterite aggregates at 1000°C–1300°C and 0.1 MPa to 10 GPa. J. Geophys. Res. 99, 19809–19819.

Fisler, D.K., Mackwell, S.J., Petsch, S., 1997. Grain boundary diffusion in enstatite. Phys. Chem. Miner. 24, 264–273.

Frost, H.J., Ashby, M.F., 1982. In: Deformation-mechanism map. Pergamon, Oxford, pp. 16–26, Chap. 2.

Garnero, E.J., Lay, T., 1997. Lateral variations in lowermost mantle shear wave anisotropy beneath the north Pasific and Alaska. J. Geophys. Res. 102, 8121–8135.

Gibbs, G.V., Hill, F.C., Boisen, M.B., Downs, R.T., 1998. Power law relationships between bond length, bond strength and electron density distributions. Phys. Chem. Miner. 25, 585–590.

Giletti, B.J., Semet, M.P., Yund, R.A., 1978. Studies in diffusion: III. Oxygen in feldspars: an ion microprobe determination. Geochim. Cosmochim. Acta 42, 45–57.

Gordon, R.S., 1985. Diffusional creep phenomena in polycrystalline oxides. In: Schock, R.N. (Ed.), Point Defects in Minerals. Geophys. Monogr. Ser. 31 AGU, Washington, DC, pp. 132–140.

Harrison, L.G., 1961. Influence of dislocations on diffusion kinetics in solids with particular reference to the alkali halides. Trans. Faraday Soc. 57, 1191–1199.

Houlier, B., Cheraghmakani, M., Jaoul, O., 1990. Silicon diffusion in San Carlos olivine. Phys. Earth Planet. Inter. 62, 329–340.

Ito, E., Takahashi, E., 1989. Postspinel transition in Mg_2SiO_4–Fe_2SiO_4. J. Geophys. Res. 94, 10637–10646.

Jaoul, O., Béjina, F., Élie, F., Abel, F., 1995. Silicon self-diffusion in quartz. Phys. Rev. Lett. 74 (11), 2038–2041.

Jaoul, O., Houlier, B., Abel, F., 1983. Study of ^{18}O diffusion in magnesium orthosilicate by nuclear microanalysis. J. Geophys. Res. 88, 613–624.

Jaoul, O., Poumellec, M., Froidevaux, C., Havette, A., 1981. Silicon diffusion in forsterite: a new constraint for understanding mantel deformation. In: Stacey, F.D. (Ed.), Anelasticity in the Earth. Godyn. Ser. Vol. 4 AGU, Washington, DC, pp. 95–100.

Karato, S. et al., 1988. The role of recrystallization in the preferred orientation of olivine. Phys. Earth Planet. Inter. 51, 107–122.

Karato, S., Li, P., 1992. Diffusion creep in perovskite: implications for the rheology of the lower mantle. Science 255, 1238–1240.

Karato, S., Zhang, S., Wenk, H.R., 1995. Superplasticity in earth's lower mantle: evidence from seismic anisotropy and rock physics. Science 270, 458–461.

Le Claire, A.D., 1963. The analysis of grain boundary diffusion measurements. Br. J. Appl. Phys. 14, 351–356.

Li, P., Karato, S., Wang, Z., 1996. High-temperature creep in fine-grained polycrystalline $CaTiO_3$, an analogue material of (Mg, Fe)SiO_3 perovskite. Phys. Earth Planet. Inter. 95, 19–36.

Lloyd, G.E., Hall, M.G., Cockayne, B., Jones, D.W., 1981. Selected-area electron-channeling patterns from geological materials: specimen preparation, indexing and representation of patterns and applications. Can. Mineral. 19, 505–518.

McCammon, C., 1997. Perovskite as a possible sink for ferric iron in the lower mantle. Nature 387, 694–696.

Meade, C., Silver, P.G., Kaneshima, S., 1995. Laboratory and seismological observations of lower mantle isotropy. Geophys. Res. Lett. 22, 1293–1296.

Ohtani, E., Suzuki, A., Kato, T., 1998. Flotation of olivine and diamond in mantle malt at high pressure: its implications for fractionation in the deep mantle and ultradeep origin of diamond. In: Manghnani, M.H., Yagi, T. (Eds.), Properties of Earth and Planetary Materials at High Pressure and Temperature. Geophys. Monogr. Ser. 101 AGU, Washington, D.C, pp. 227–239.

Raj, R., Ashby, M.F., 1971. On grain boundary sliding and diffusional creep. Metall. Trans. 2, 1113–1127.

Ren, S.X., Kenik, E.A., Alexander, K.B., Goyal, A., 1998. Exploring spatial resolution in electron back-scattered diffraction experiments via Monte Carlo simulation. Microsc. Microanal. 4, 15–22.

Ricoult, D.L., Kohlstedt, D.L., 1983. Structural width of low-angle grain boundaries in olivine. Phys. Chem. Miner. 9, 133–138.

Sakaguchi, I., Haneda, H., 1996. Oxygen tracer diffusion in single-crystal $CaTiO_3$. J. Solid State Chem. 124, 195–197.

Stixrude, L., Hemly, R.J., Fei, Y., Mao, H.K., 1992. Thermoelasticity of silicate perovskite and magnesiowüstite and stratification of the earth's mantle. Science 257, 1099–1101.

Stocker, R.L., Ashby, M.F., 1973. On the rheology of the upper mantle. Rev. Geophys. 11, 391–426.

Turnbell, D., Hoffman, R.E., 1954. The effect of relative crystal and boundary orientations on grain boundary diffusion rates. Acta Metall. 2, 419–426.

Wood, B.J., Rubie, D.C., 1996. The effect of alumina on phase transformations at the 660-kilometer discontinuity from Fe–Mg partitioning experiments. Science 273, 1522–1524.

Yurimoto, H., Morioka, M., Nagasawa, H., 1992. Oxygen self-dif-

fusion along high diffusivity paths in forsterite. Geochem. J. 26, 181–188.

Yurimoto, H., Morioka, M., Nagasawa, H., 1989. Diffusion in single crystals of melilite. I: Oxygen. Geochim. Cosmochim. Acta. 53, 2387–2394.

Yurimoto, H., Sueno, S., 1984. Anion and cation partitioning between olivine, plagioclase phenocrysta and the host magmas: A new application of ion microprobe study. Geochem. J. 18, 85–94.